Secreted osteopontin from CD4+ T cells limits acute graft-versus-host disease

Nupur Aggarwal[1,4], **M. Elizabeth Deerhake**[1,4], **Devon DiPalma**[1], **Shailesh K. Shahi**[2], **Margaret R. Gaggioli**[3], **Ashutosh K. Mangalam**[2], **Mari L. Shinohara**[1,3,5,*]

[1]Department of Immunology, Duke University Medical School, Durham, NC 27710, USA

[2]Department of Pathology, University of Iowa, Iowa City, IA 52242, USA

[3]Department of Molecular Genetics and Microbiology, Duke University Medical School, Durham, NC 27710, USA

[4]These authors contributed equally

[5]Lead contact

SUMMARY

Osteopontin (OPN) has been considered a potential biomarker of graft-versus-host disease (GVHD). However, the function of OPN in GVHD is still elusive. Using a mouse model of acute GVHD (aGVHD), we report that OPN generated by CD4+ T cells is sufficient to exert a beneficial effect in controlling aGVHD through limiting gastrointestinal pathology, a major target organ of aGVHD. CD4+ T cell-derived OPN works on CD44 expressed in intestinal epithelial cells (IECs) and abates cell death of IECs. OPN also modulates gut microbiota with enhanced health-associated commensal bacteria *Akkermansia*. Importantly, we use our *in vivo* mouse mutant model to specifically express OPN isoforms and demonstrate that secreted OPN (sOPN), not intracellular OPN (iOPN), is solely responsible for the protective role of OPN. This study demonstrates that sOPN generated by CD4+ T cells is potent enough to limit aGVHD.

Graphical abstract

Allogeneic CD4+ T cell-mediated acute GVHD

In brief

The role of osteopontin (OPN) derived from CD4+ T cells in acute graft-versus-host disease (aGVHD) is unknown. Aggarwal et al. show that CD4+ T cell-derived secreted OPN is protective in aGVHD by modulating the gut microbiome and limiting cell death of intestinal epithelial cells by the sOPN-CD44 axis.

INTRODUCTION

Allogenic hematopoietic stem cell transplantation (HSCT) is a widely used treatment for hematological malignancies, some solid tumors, and immune deficiency-related diseases. HSCT involves the transfer of healthy bone marrow (BM) stem cells into patients with either dysfunctional or depleted BM cells by radiation or chemotherapy. The major complication of HSCT is graft-versus-host disease (GVHD). During GVHD, donor allogeneic T cells target and attack organs or tissues of the recipients, such as skin, liver, and gut. These reactions can be categorized into chronic GVHD (cGVHD) or acute GVHD (aGVHD) depending on the time of clinical presentation, distinct histopathology, and pathophysiology. aGVHD is predominantly mediated by T helper (T_H) 1 and T_H17 immune responses, whereas cGVHD exhibits T_H1, T_H2, and T_H17 responses (Allen et al., 1993; Coghill et al., 2011; Shlomchik et al., 2007; Via et al., 1994; Zeiser and Blazar, 2017). Conditioning regimens before HSCT also induce damage to gut epithelial cells, prompting the translocation of microbial products into the circulation and allowing them to bind to

pattern-recognition receptors (PRRs) to stimulate cytokine production, which favors GVHD (Ghimire et al., 2017; Hong et al., 2021; MacDonald et al., 2017).

Osteopontin (OPN), also known as secreted phosphoprotein-1 (*Spp1*) and early T lymphocyte activation-1 (Eta-1), is expressed by various cell types, such as epithelial cells; endothelial cells; and immune cells, such as T cells, B cells, macrophages, neutrophils, and dendritic cells. Elevated OPN expression is often identified in various conditions associated with inflammation; thus, OPN is generally considered a pro-inflammatory molecule (Inoue and Shinohara, 2011; Jansson et al., 2002; Patouraux et al., 2012; Uede, 2011; Vaschetto et al., 2008). OPN exists as two different isoforms: secreted OPN(sOPN) and intracellular OPN(iOPN) produced by alternative translation (Shinohara et al., 2008). sOPN binds multiple integrins, including $\alpha v\beta 3$, $\alpha v\beta 1$, $\alpha v\beta 5$, $\alpha v\beta 6$, $\alpha 5\beta 1$, $\alpha 8\beta 1$, $\alpha 9\beta 1$, $\alpha 4\beta 1$, and $\alpha 4\beta 7$ (Barry et al., 2000a, 2000b; Denhardt and Noda, 1998; Gladson and Cheresh, 1991; Inoue and Shinohara, 2011). Besides integrins, the C terminus of sOPN binds to CD44 (Ashkar et al., 2000). sOPN is involved in regulating T_H cell polarization and macrophage cytokine production during the immunologic process, and promotes cell survival by inhibiting apoptosis (Ashkar et al., 2000; Hur et al., 2007; Inoue and Shinohara, 2015; Renkl et al., 2005; Scatena et al., 1998; Shinohara et al., 2005). In contrast, iOPN works as a scaffold protein in various intracellular signal transduction pathways (Inoue et al., 2011, 2014; Kanayama et al., 2017; Leavenworth et al., 2015a, 2015b; Shinohara et al., 2006). Thus, sOPN and iOPN have different functions due to their distinct localizations, inside or outside of cells. The separation of OPN isoforms is a challenge because they are translational isoforms, and the alternative translation site is located proximally at the 3′ end of the signal sequence encoding region (Shinohara et al., 2008). Thus, the separation between iOPN and sOPN simply by their sizes on western blotting is not reliable.

Multiple clinical studies have indicated OPN as a biomarker of GVHD diagnosis and disease severity (Paczesny, 2018; Wolff et al., 2018; Yu et al., 2016), but the role of OPN in GVHD is still elusive. For example, two previous studies using animal GVHD models showed opposing roles of OPN (Kawakami et al., 2017; Zhao et al., 2011). It is also not clear which cell types affect GVHD and which OPN isoform is the effector. In this study, we focused on damage in the gastrointestinal (GI) tract, a major target organ of aGVHD, and how the integrity of the GI tract influences the severity and progression of aGVHD (Hill and Ferrara, 2000). Our novel mouse *in vivo* system demonstrated that sOPN derived from donor CD4+ T cells is sufficient to elicit a protective role in GI aGVHD by limiting T cell infiltration and cell death of intestinal epithelial cells (IECs). In addition, CD4+ T cell-derived sOPN provides a host-beneficial pattern of gut microbiota.

RESULTS

Protective role of OPN in allogeneic CD4+ T cells in aGVHD

The role of OPN in donor CD4+ T cells has not been studied in GVHD, although CD4+ T cells are suggested to be responsible for GI injuries (Korngold, 1993). Thus, we validated the pathogenicity of allogeneic CD4+ T cells by comparing allogeneic (B6) versus syngeneic (BALB/c) CD4+ T cell transfer (accompanied by T cell-depleted B6 BM cells) to BALB/c recipients. All the genotypes are $Spp1^{-/-}$ in this experiment. Recipients of allogeneic

B6 CD4$^+$ T cells showed aGVHD with severe weight loss, clinical signs evaluated with clinical scores, and diarrhea in a majority of mice, while recipients of BALB/c syngeneic CD4$^+$ T cells did not show signs of aGVHD (Figures S1A–S1D). The data suggested the pathogenicity of allogeneic CD4$^+$ T cells in the aGVHD model. Next, we compared the impact of OPN derived by donor CD4$^+$ T cells by adoptively transferring wild-type (WT) or *Spp1$^{-/-}$* B6 CD4$^+$ T cells (along with total T cell-depleted B6 *Spp1$^{-/-}$* BM cells) to irradiated *Spp1$^{-/-}$* BALB/c recipients (Figure 1A). *Spp1$^{-/-}$* CD4$^+$ T donor cells induced severe aGVHD with greater weight loss (Figure 1B), more severe clinical scores (Figure 1C), and reduced survival (Figure 1D) compared with recipients of WT CD4$^+$ T donor cells. *Spp1$^{-/-}$* CD4$^+$ T cell recipients showed severe pathology in the colon and the small intestine (SI), such as blunted villi, loss and regeneration of crypts, and statistically significantly high histological scores (Figures 1E–1G), compared with recipients of WT CD4$^+$ T cells. These results suggested that OPN derived from CD4$^+$ T donor cells is protective in aGVHD.

Because the setting shown in Figure 1 had *Spp1$^{-/-}$* BALB/c recipients, we also evaluated aGVHD with WT BALB/c recipients (Figure 2A). Here also, recipients of WT CD4$^+$ T cells had less weight loss (Figure 2B) and lower clinical scores (Figure 2C) than recipients of *Spp1$^{-/-}$* CD4$^+$ T cells. Thus, the impact of CD4$^+$ T cell-derived OPN was not masked even with OPN derived from recipients, suggesting that CD4$^+$ T cell-derived OPN is critical in limiting aGVHD. Furthermore, we compared the impact of recipient-derived OPN (Figure 2D). The results indicated that recipient-derived OPN contributed to slightly less weight loss (Figure 2E), but the change in mouse survival did not reach statistical significance (Figure 2F). The results here strongly suggest that OPN generated by allogeneic CD4$^+$ T cells is beneficial in aGVHD. Of note, the protective role of CD4$^+$ T cell-derived OPN is significant enough to surpass that of OPN derived from recipient cells. Based on the clear impact of OPN, we used *Spp1$^{-/-}$* T cell-depleted BM cells and *Spp1$^{-/-}$* recipients hereafter in experiments described below to exclude the participation of OPN released by cells other than CD4$^+$ T cells unless otherwise noted.

No impact of OPN on naive CD4$^+$ T cell composition and allogeneic CD4$^+$ T cell proliferation

We next sought to determine if OPN alters donor CD4$^+$ T cell phenotypes. *Spp1$^{-/-}$* CD4$^+$ T cells before transfer showed a subset composition comparable with WT CD4$^+$ T cells in T_H1, T_H17, and regulatory T cells (T_{regs}) (Figures S2A and S2B). Next, we sought to determine whether OPN can limit T cell proliferation using a mixed lymphocyte reaction (MLR) by coculturing BALB/c splenocytes with B6 CD4$^+$ T cells. Two previous studies demonstrated that treatment with recombinant OPN (rOPN) slightly enhanced MLR using human peripheral blood mononuclear cells (Kaleta, 2019; Renkl et al., 2005), but we did not observe the effect of OPN in *ex vivo* CD4$^+$ T cell proliferation (Figure S2C). These results suggested no apparent impact of OPN on the composition of pre-transferred CD4$^+$ T cells and allogeneic CD4$^+$ T cell proliferation.

No changes in leukocyte composition and systemic immunophenotypes with T cell-derived OPN

To determine how OPN mediates its protective function *in vivo* in aGVHD, we evaluated immune cell subsets in the colon and SI of recipients that received WT or $Spp1^{-/-}$ CD4$^+$ T cells, by flow cytometry (gating strategy in Figure S3A). We specifically evaluated the gut at the disease peak on day 7 post transplant. Increased total and effector (CD44$^+$CD62L$^-$) CD4$^+$ T cells were observed when CD4$^+$ T cells were $Spp1^{-/-}$ in both the SI (Figures 3A and 3B) and colon (Figures 3C and 3D). (Because almost all the CD4$^+$ T cells in the colon are effector cells, Figures 3C and 3D look similar.) We further evaluated T$_H$ subsets in the colon, but the numbers of T$_H$1, T$_H$17, and T$_{reg}$ cells were similar between groups that received WT or $Spp1^{-/-}$ CD4$^+$ T cells (Figure 3E). In contrast to reduced CD4$^+$ T cell numbers in the WT CD4$^+$ T cell-transferred group, myeloid cell numbers were comparable in SI and colon (Figures S3B and S3C). The distribution of CD4$^+$ T cells and CD68$^+$ cells also exhibited no apparent difference in the SI and colon between recipients of WT or $Spp1^{-/-}$ CD4$^+$ T cells (Figures S3D–S3G). In addition, levels of mRNA for chemokines and cytokines (*Cxcl10, Ccl2, Ccl3, Ccl20, Cx3cl1*, and *Il18*) in the SI did not show differences between the two groups (Figure S3H). Expression levels of the *Ifng, Il1b, Il6, Il17*, and *Tnfa* were too low to be evaluated.

We also evaluated the spleen in aGVHD mice. No statistically significant changes in total and effector CD4$^+$ T cells were found between recipients transferred with WT versus $Spp1^{-/-}$ CD4$^+$ T cells (Figures S4A and S4B). Similarly, there were no significant differences in numbers of Ly6G$^+$ neutrophils, Ly6C^{hi} monocytes, and F4/80^{hi} macrophages (Figure S4C). Serum inflammatory cytokine levels (interferon-gamma [IFN-γ], Monocyte chemoattractant protein-1 [MCP-1], interleukin [IL]-10, IL-6, IL-27, IL-1α, IL-1β, and tumor necrosis factor alpha [TNF-α]) were also comparable (Figures S4D–S4F). These results suggest that CD4$^+$ T cell-derived OPN limits T cell infiltration in the gut without affecting the T$_H$ cell subset composition and major systemic immunophenotypes.

OPN not acting on CD4$^+$ T cells in a cell-intrinsic manner but limiting cell death in SI

Because OPN limited the number of donor CD4$^+$ T cells in the colon and SI in aGVHD, we next asked whether CD4$^+$ T cell-derived OPN acts in a cell-intrinsic manner to restrict migration, proliferation, or survival. To test this, we evaluated $Spp1^{-/-}$ recipients that had received a 50/50 mixture of B6 WT (CD45.1) and $Spp1^{-/-}$ (CD45.2) CD4$^+$ T cells (Figure S4G), along with T cell-depleted $Spp1^{-/-}$ BM cells. Despite a weak trend of slightly more WT CD4$^+$ T cells, we did not observe significant differences in the relative frequency of WT and $Spp1^{-/-}$ CD4$^+$ cells in the colon, SI, spleen, or mesentric lymph node (MLN) on day 7 post transfer (Figure S4H). This suggests that OPN does not significantly limit donor CD4$^+$ T cell numbers in a cell-intrinsic manner. In addition, relative frequencies of proliferating (Ki67$^+$) (Figure S4I) and apoptotic cells (Figure S4J) post transfer were also comparable between WT and $Spp1^{-/-}$ donor CD4$^+$ T cells in the colon, SI, spleen, or MLN.

Next, we sought to identify phenotypes of aGVHD pathogenesis without OPN in transferred CD4$^+$ T cells. Using the model transferring either WT versus $Spp1^{-/-}$ CD4$^+$ T cells (Figure 1A), we found higher numbers of TUNEL$^+$ cells in the SI of $Spp1^{-/-}$ CD4$^+$ T cell recipients

than WT CD4^{+} T cell recipients (Figures 3F–3J). In sum, CD4^{+} T cell-derived OPN does not change the intrinsic phenotype of CD4^{+} T cells but limits aGVHD by reducing cell death. The impact of OPN is apparent in the SI.

Effect of T cell-derived OPN on the epithelium-microbiome axis during aGVHD

Given the importance of epithelium-microbiota interactions in the gut, we next investigated how OPN may be influencing this axis by evaluating the microbiome using bacterial 16S gene sequencing in fecal samples. First, we identified that mice with aGVHD have distinct microbiota from naive and irradiated mice (Figure 4A). The Shannon diversity index further indicated that aGVHD mice had reduced microbial diversity (Figure 4B). Furthermore, Lactobacillales and Enterobacteriales bacteria were enriched in aGVHD mice (Figure 4C). At the genus level, *Escherichia* (in the Enterobacteriales order) was increased in GVHD mice compared with naive and irradiated mice (Figure 4D). This observation correlates with previous studies where the GVHD microbiome is characterized by a loss of microbial diversity and an overabundance of the *Escherichia* genus (Chiusolo et al., 2015; Heimesaat et al., 2010; Holler et al., 2014). However, OPN did not appear to regulate these features of the GVHD-associated microbiome. Instead, we found that OPN greatly enhanced the levels of health-associated commensal bacteria *Akkermansia* (in the Clostridiales order) (Figure 4E). Lower levels or loss of *Akkermansia* have been associated with an increased risk of developing aGVHD (Ilett et al., 2020). In contrast, OPN from CD4^{+} T cells significantly reduced the overall levels of commensal bacteria of the Bacteroidales order (Figure 4F). The reduction with OPN is reflected in the trend of major genera of Bacteroidales, such as *Bacteroides* and *S24-7* (also known as Muribaculaceae) (Figure 4G).

Next, we evaluated the gene expression in hosts SI and found that the expression of *Defa5* (encoding a host anti-microbial peptide DEFA5, alpha-defensin 5) was higher in mice with *Spp1*^{−/−} CD4^{+} T cells (Figure 4H). Epithelial cells are known to regulate the abundance of bacteria in the Bacteroidetes phylum through the expression of DEFA5 (Ou et al., 2020). Paradoxically, DEFA5 does not exhibit anti-microbial activity against Bacteroidetes, but it promotes adherence of Bacteroidetes to IECs and elevates the relative abundance of Bacteroidetes in commensal microbiota (Ou et al., 2020). Indeed, the trend of gene expression in the SI of *Spp1*^{−/−} CD4^{+} T cell recipients was increased *Defa5*, as well as Pan-cryptidin transcripts encoding anti-microbial defensins (Figure 4H). These increases may be reflecting the pathogenic gut microbial environment in *Spp1*^{−/−} CD4^{+} T cell recipients. We also evaluated bacteria residing in the SI using qPCR. As shown in fecal samples, OPN also limited the abundance of Bacteroidetes and Firmicutes phyla in the SI (Figure 4I). Together, these results suggest a model in which T cell-derived OPN regulates the epithelium-microbiome axis during GVHD by inhibiting apoptosis and allowing low *Defa5* expression in IECs, resulting in reduced levels of epithelium-associated Bacteroidetes and increased commensal bacteria, *Akkermansia*.

Secreted OPN, but not intracellular OPN, is protective

As OPN is protective, we sought to identify if the mechanism is attributed to sOPN or iOPN using our new mouse genetics system to express sOPN or iOPN specifically. In this study, we generated a Lox-STOP-Lox (LSL)-sOPN mouse line, which enables the expression

of sOPN alone under Cre expression. (The mouse line expressing iOPN, LSL-iOPN, has already been described in our previous study; Kanayama et al., 2017). sOPN is generated by the canonical AUG translation start codon, and its nascent protein includes a signal sequence that targets sOPN to the ER/Golgi for secretion. In contrast, the iOPN isoform is generated by alternative translation at a non-AUG alternative start codon located at the 3′-proximal end of *Spp1* signal sequence transcript (Shinohara et al., 2008). Thus, the nascent iOPN protein does not include signal sequence and stays in the cytoplasm (Shinohara et al., 2008). However, it appears that the *Spp1* signal sequence transcript is somehow essential for initiating alternative translation (Inoue and Shinohara, 2011); thus, the complete removal of *Spp1* signal sequence (45 nt) abolishes the production of not only sOPN but iOPN too (Kanayama et al., 2017; Shinohara et al., 2005, 2006, 2008; Singh et al., 2017). Based on this information, we sought to generate sOPN alone by replacing the *Spp1* signal sequence (45 nt) with the *Il2* signal sequence (57 nt) (Figures 5A and S5A) (Sasada et al., 1988; Smith et al., 1985). Of note, mature OPN generated by this approach does *not* include IL-2 amino acid sequence because the IL-2 signal sequence is cleaved immediately after translation. Replacement of the *Spp1* signal sequence to the *Il2* signal sequence was confirmed in the mice possessing the LSL-sOPN homozygous mutant (Figures S5B and S5C). In LSL-sOPN mice without Cre expression, the mice do not express either sOPN or iOPN. LSL-sOPN;*Vav1^{Cre}* mice express sOPN alone in all the hematopoietic cells. To validate the specific production of sOPN in LSL-sOPN;*Vav1^{Cre}* mice, we used BM-derived macrophages (BMDMs), rather than T cells, to better visualize the subcellular compartments. First, LSL-sOPN;*Vav1^{Cre}* cells successfully released sOPN to tissue culture supernatants at levels comparable with WT cells, while no sOPN was detected from cells with LSL-sOPN without Cre (Figure 5B). Furthermore, we confirmed the absence of iOPN in the cytosol of LSL-sOPN; *Vav1^{Cre}* and LSL-sOPN cells, while iOPN was identified in the cytosol of WT cells (Figure 5C). Immunofluorescence staining also confirmed the localization of sOPN in the Golgi in LSL-sOPN;-*Vav1^{Cre}* cells but no OPN in LSL-sOPN cells (Figure 5D).

Using this new mouse system, we examined which T cell-derived OPN isoform, sOPN or iOPN, controls aGVHD. To do so, we first tested sOPN using LSL-sOPN versus LSL-sOPN;*Vav1^{Cre}* donor CD4$^+$ T cells. The recipients of LSL-sOPN;*Vav1^{Cre}* CD4$^+$ T cells had lower weight loss and more remarkable survival than recipients of LSL-sOPN mice CD4$^+$ T cells (Figures 5E and 5F). In contrast, no difference was found in recipients of LSL-iOPN; *Vav1^{cre}* versus LSL-iOPN mice CD4$^+$ T cells (Figures 5G and 5H). We further evaluated T$_H$ subsets in the colon and spleen in aGVHD mice, but there was no significant difference in T$_H$1, T$_H$17, and T$_{reg}$ cells among recipient groups that received CD4$^+$ T cells expressing either sOPN, iOPN, or no OPN at all (Figures S5D and S5E). The results indicate that sOPN, derived from CD4$^+$ T cells, is beneficial in aGVHD without affecting T cell polarization.

IECs in aGVHD mice highly express CD44, an sOPN receptor

To determine whether IECs express cell surface OPN receptors during aGVHD, we examined gene expression in IECs isolated from naive and aGVHD tissues. Specifically, we looked at IECs 3 days after GVHD induction to identify which receptors are poised to

respond to CD4^{+} T cell-derived sOPN and mediate its beneficial function. Among a panel of 12 candidate genes (*Itgav*, *Itgax*, *Itga4*, *Itga5*, *Itga8*, *Itga9*, *Itgb1*, *Itgb2*, *Itgb3*, *Itgb5*, *Itgb6*, *Cd44*), we found that IECs expressed detectable levels of *Cd44*, *Itgb1*, *Itgb6*, and *Itgav* transcripts from the SI and colon (Figures S6A and S6B). Of these, *Cd44* was the only gene upregulated during aGVHD (Figure S6A). Furthermore, immunofluorescent images showed that CD44 was highly expressed in IECs both in naive and aGVHD mice (Figures S6C and S6D). Here, we conclude that CD44 on IEC could be a potential candidate receptor detecting sOPN.

Protection of IECs from cell death by the sOPN-CD44 axis

A previous article reported OPN-deficient mice showing mild but statistically significant reduction of occludin expression in naive mice and mice with DSS colitis (Woo et al., 2019). Thus, we evaluated the expression of genes encoding occludin, claudin-1, and tight junction protein-1 in SI between aGVHD induced with WT versus *Spp1*^{−/−} CD4^{+} T cells, but no evident change was observed (Figure S7A). We also did not identify a difference between the two groups of mice in the epithelial integrity evaluated by an intestinal permeability assay using FITC-dextran (Figure S7B) and endotoxin breaching into the circulation (Figure S7C). Therefore, we ruled out a clear impact of OPN on tight junctions or intestinal permeability *in vivo* during aGVHD. Thus, it is possible that sOPN works directly on IECs through CD44 to protect them from cell death because CD44 is known to promote epithelial cell proliferation and survival in the SI and colon under homeostatic conditions (Riehl et al., 2015).

Because results in Figures 3F–3J suggested that recipients transferred with *Spp1*^{−/−} CD4^{+} T cells showed increased cell death during aGVHD, we assessed the impact of sOPN through CD44 on IEC survival using precision-cut intestinal slices (PCIS) to evaluate if recombinant OPN (rOPN) protects IECs from cell death in live tissue slices. The SI tissue slices were from *Spp1*^{−/−} mice to rule out sOPN from tissues, and cell death was induced with TNFα with or without a CD44 blocking antibody (Figures 6A–6D). With TUNEL staining, the result indicated that rOPN protects IECs from cell death but the blockade of CD44 abrogated the protective effect of rOPN (Figures 6C–6E). Taken together, rather than enhancing tight-junction-gene expression, sOPN works on IECs through CD44 to protect them from cell death.

DISCUSSION

Multiple clinical studies indicated OPN as a biomarker of GVHD diagnosis (Paczesny, 2018; Wolff et al., 2018; Yu et al., 2016), but the role of OPN in GVHD was still not clear. In this study, we found that the sOPN isoform produced by donor CD4^{+} T cells is potent and sufficient to ameliorate GI-aGVHD by protecting IECs from cell death and limiting intestinal inflammation, reflected in gut microbiota. sOPN from T cells is generally known for its pro-inflammatory functions in promoting CD4^{+} T cell survival, migration, and T$_H$ subset differentiation (Hur et al., 2007; Inoue and Shinohara, 2015; Shinohara et al., 2005). Thus, the beneficial role of T cell-derived OPN in GVHD is seemingly counter-intuitive.

Previous studies on animal GVHD models used OPN-sufficient (WT) recipients (Kawakami et al., 2017; Zhao et al., 2011); thus, all tested mice had sOPN, unless OPN was neutralized. Here, we used a more precise approach by (1) using $Spp1^{-/-}$ recipient mice (we backcrossed $Spp1^{-/-}$ mice to BALB/c for 14 generations) and $Spp1^{-/-}$ T cell-depleted BM cells to exclude background sOPN, (2) focusing the impact of OPN on donor B6 CD4$^+$ T cells obtained from genetically modified mice, and (3) clearly distinguishing two OPN isoforms by using a new mouse genetic model system.

The two previous animal model studies strongly suggested the involvement of OPN in GVHD. However, the studies showed an apparent discrepancy in the results; Kawakami et al. (2017) demonstrated OPN as beneficial, while Zhao et al. (2011) showed OPN to be detrimental. Kawakami et al. (2017) compared WT with OPN KO donor cells, consisting of total BM cells and total splenocytes, and showed OPN's protective role in the gut, reflecting the results of our study. Although they found OPN-mediated Fas-ligand downregulation in CD8$^+$ T cells, the *in vivo* experimental setting is not CD8$^+$ T cell specific, and no significant change in epithelial cell death was found with their approach (Kawakami et al., 2017). In contrast, Zhao et al. (2011) showed that OPN neutralizing antibody treatment ameliorated GVHD in irradiated WT recipients, transferred with WT CD8$^+$ T cells and T cell-depleted BM. They did not use genetically modified mice; thus, OPN Ab was administered five times between days 0 and 14 to demonstrate the phenotype (Zhao et al., 2011). Therefore, the result by Zhao et al. also suggests the involvement of sOPN, although they concluded that OPN was detrimental. Here, the question is what led to the discrepancy (i.e., OPN as detrimental or beneficial in GVHD). There may be multiple explanations, but a clear difference is the extent of disease intensity and acuteness. The experimental setting used by Zhao et al. is milder than the settings by Kawakami et al. and ours. Based on Zhao et al.'s results, weight loss on day 7 was mild, and mouse evaluation was performed at a late time point (on day 35), which suggests a more chronic aspect in their disease (Kawakami et al., 2017; Zhao et al., 2011). In our previous study of colitis triggered by chronic lymphopenia-induced proliferation (cLIP), sOPN turned out to be detrimental by enhancing the migration of T cells to the colon and skewing the T cell immunity toward $T_H 1$ (Kanayama et al., 2017), which we did not observe in this aGVHD study. In the chronic condition of cLIP, mice showed slight weight loss and took 1 month to identify a clear phenotype (Kanayama et al., 2017). Taken all together with more studies using colitis models (Heilmann et al., 2009; Kourepini et al., 2014), OPN may be protective when the intestinal inflammation is acute and severe, but OPN may function as a detrimental molecule with chronic and mild intestinal inflammation (da Silva et al., 2009; Da Silva et al., 2006; Heilmann et al., 2009; Kourepini et al., 2014). That said, the seemingly contradicting result by Zhao et al. could make sense due to the distinct kinetics in disease progression, and the role of OPN may indeed be two faced depending on whether the setting is acute or chronic.

We demonstrated that recipients with $Spp1^{-/-}$ CD4$^+$ T cells had more infiltration of CD4$^+$ T cells in SI and the colon than recipients with WT CD4$^+$ T cells. However, no difference was found between WT and $Spp1^{-/-}$ CD4$^+$ T cells when mixed and transferred to recipients. Therefore, OPN generated by CD4$^+$ T cells does not limit their infiltration in the gut in a cell-intrinsic or autocrine manner. The dataset also supported our results using iOPN-expression-specific mice, which ruled out the impact of iOPN in our finding. Instead, sOPN

is attributed to the protective role in aGVHD. sOPN is well characterized as a CD44 ligand, and we demonstrated that the sOPN-CD44 axis exerted a beneficial effect by limiting cell death of IECs. Indeed, the anti-apoptotic role of the sOPN-CD44 axis has been previously reported by another group (Lee et al., 2007). Here, CD44 expression was identified in crypt epithelial cells from both naive and aGVHD mice. Thus, sOPN provided by CD4$^+$ T cells is sufficient for the protective phenotype without inducing CD44 expression in the colon.

In our study, we found a significant increase in the abundance of Bacteroidetes with $Spp1^{-/-}$ CD4$^+$ T cell transfer, as shown both in fecal samples and SI tissues. Whether this directly affects the lack of sOPN-CD44 interaction or indirectly increases epithelial damage remains to be determined. Although Bacteroidetes are physiologic commensals, we hypothesize that the increased burden of specifically epithelium-associated Bacteroidetes may exacerbate inflammation in the setting of intestinal barrier damage during GVHD. Interactions between epithelial cells, the microbiome, and the immune system are increasingly important in the pathogenesis of acute GVHD. In particular, understanding the mechanisms behind the effect of T cell-derived sOPN on the immune-epithelial interaction could provide new insight on how to modulate the microbiome to limit host tissue damage following HSCT.

OPN is a potential biomarker associated with GVHD and complications post HSCT in patients (Yu et al., 2016), including bronchiolitis obliterans syndrome post allogenic HSCT (Williams et al., 2016). However, our findings provoke a reconsideration of OPN function in GVHD, and future therapeutic approaches targeting OPN should take into account both its potential beneficial and detrimental functions, particularly in the setting of intestinal inflammation. Furthermore, understanding the mechanisms of sOPN regulation of epithelium-microbial interactions will also merit further investigation and may potentially be a therapeutic approach for protecting the GI tract in the setting of aGVHD.

Limitations of the study

This study identified a protective role of CD4$^+$ T cell-derived sOPN in aGVHD by reducing IEC death via CD44 on IECs. However, protective mechanisms other than the sOPN-CD44 axis through IECs may be involved. Using mixed WT and $Spp1^{-/-}$ CD4$^+$ T cells, we also demonstrated that OPN did not modify CD4$^+$ T cell migration, proliferation, and apoptosis. Although this approach rules out the impact of cell-intrinsic OPN, i.e., iOPN, it is still possible that sOPN alters the outcomes. The caveat of the experiment is that both WT and $Spp1^{-/-}$ CD4$^+$ T cells are surrounded by sOPN generated by WT CD4$^+$ T cells.

STAR★METHODS

RESOURCE AVAILABILITY

Lead contact—Further information and requests for resources and reagents should be directed to and will be fulfilled by the Lead Contact, Mari L. Shinohara, PhD (mari.shinohara@duke.edu).

Materials availability—This study generated the new LSL-sOPN mouse line in the Shinohara laboratory.

Data and code availability

- Bacterial sequence data has been deposited at NCBI under the accession number: PRJNA731868.

- This paper does not report original code.

- Any additional information required to reanalyze the data reported in this paper is available from the lead contact upon request.

EXPERIMENTAL MODEL AND SUBJECT DETAILS

Mice—C57BL/6J (B6) (JAX#000664), BALB/cJ (JAX#000651), B6 $Spp1^{-/-}$ (JAX#004935), B6 $Vav1^{cre}$ (JAX #008610), and B6 CD45.1 (JAX #002014) mice were purchased from Jackson Laboratory. BALB/c $Spp1^{-/-}$ mice were obtained by backcrossing 129 $Spp1^{-/-}$ mice to BALB/cJ for at least 14 generations by us. B6 LSL-iOPN (Kanayama et al., 2017) and B6 LSL-sOPN mice were created in our laboratory and were crossed with $Vav1^{cre}$ mice to generate LSL-iOPN;$Vav1^{cre}$ and LSL-sOPN;$Vav1^{cre}$. Mice aged 8-12 weeks were used for all the experiments. Mice were sex-matched, and no differences in results between male and female mice were found. All mouse procedures were approved by the Institutional Animal Care and Use Committee at Duke University and housed in a specific pathogen-free facility.

METHOD DETAILS

Preparation of T cell-depleted bone marrow cells and CD4$^+$ T cells—BM cells were flushed from the femur and tibia of hind legs of naive mice using phosphate buffer saline (PBS) and 2% FCS followed by RBC lysis. Freshly prepared BM cells were negatively selected by streptavidin magnetic beads (Miltenyi Biotec) with biotin-conjugated anti-CD3, anti-CD4, and anti-CD8 antibodies (listed in key resources table). CD4$^+$ T cells were obtained from the spleen of naive mice using Mouse CD4 T Lymphocyte Enrichment Set (BD biosciences), as recommended by the manufacturer.

Acute GVHD induction and disease scoring—aGVHD was induced by adoptive transfer of 10^5 donor CD4$^+$ T cells (various genotypes, Figure 1A) into lethally irradiated (750 rads; XRAD 320 X-Ray irradiator) BALB/c recipient mice along with 5×10^6 T cell-depleted BM cells from naive B6 $Spp1^{-/-}$ mice. Unless otherwise specified, we used the aGVHD induction method described in Figure 1A. Mice were monitored daily for weight loss, and clinical scoring was performed as previously described (Cooke et al., 1996). In some experiments, we used mixed CD45.1 WT CD4$^+$ T cells and CD45.2 $Spp1^{-/-}$ CD4$^+$ T cells (5×10^4 cells each). To distinguish between donor B6 $Spp1^{-/-}$ CD4$^+$ T cells from recipient BALB/c cells (CD45.2$^+$ for both), we used antibodies against H-2Kb and H-2Kd, respectively. Mice were monitored daily for weight loss and clinical scoring until day 7.

Intestinal leukocyte preparation—Leukocytes from the colon and SI were prepared as previously described (Liang et al., 2016). Briefly, colon and SI were removed, opened longitudinally, and gently washed with ice-cold PBS. Tissues were minced, enzymatically digested in complete RPMI 1640 medium (Thermo Fisher) with Liberase enzyme (10mg/ml; MilliporeSigma) in the presence of DNAse I (8 U/ml, SigmaAldrich), then incubated in C-

tubes (Miltenyi) with gentle agitation for 30 minutes at 37°C. After sample homogenization using GentleMACS Dissociator (Miltenyi), cells went through two-step filtration with a 100 μm mesh followed by a 40 μm mesh. Red blood cells were lysed before analysis.

Intestinal epithelial cell isolation—Intestinal epithelial cells (IECs) were isolated using previously published protocol (Zeineldin and Neufeld, 2012). Briefly, the intestine was dissected, and contents were cleaned by flushing with cold PBS. Tissues were then incubated in 0.04% sodium hypochlorite to remove bacterial contaminants, then rinsed with PBS before incubation in buffer containing DTT and EDTA. After 15 min incubation on ice, intestinal pieces were transferred to PBS and vortexed to dissociate epithelial layer cells. Incubation and mechanical dissociation were repeated twice more. Isolated cells were centrifuged onto a microscope slide using a cytocentrifuge, and IF staining with EpCAM Ab was performed to confirm the isolation of epithelial cells (data not shown). Trizol was used to prepare RNA from obtained cells.

Flow cytometry analyses—Freshly isolated cells were used for the procedures. Information on antibodies is listed in Key resources Table. Following markers were used to identify the specific population of cells; total leukocytes (CD45$^+$), neutrophils (Ly6G$^+$), monocytes/macrophages in the gut (CD64$^+$Ly6G$^-$Ly6C$^+$), splenic F4/80^{hi} macrophage (CD11b$^+$F4/80^{hi}Ly6G$^-$Ly6C$^+$), splenic monocytes (CD11b$^+$Ly6G$^-$Ly6C^{hi}), and dendritic cells (DC) (CD11c$^+$F4/80$^-$CD64$^-$). The gating strategy for the SI is shown in Fig. S3A. For intracellular cytokines staining (ICS), cells were treated with phorbol 12-myristate 13-acetate (PMA, 10 ng/ml, Sigma Aldrich) and Ionomycin (1 μg/ml, Sigma Aldrich) for 5-6 hrs with GolgiPlug (BD Biosciences) in the last 4 hrs. Cytofix/Cytoperm kit (BD Biosciences) was used for ICS. FOXP3 Fix/Perm Kit (BioLegend) was used for Foxp3 staining. Apoptotic cells were analyzed using FITC-Annexin V Apoptosis Detection Kit with 7-AAD (BioLegend) as recommended by the manufacturer. Cell proliferation was detected by Ki67 staining, where surface-stained cells were fixed and permeabilized using 70% ethanol for 1hr at −20°C followed by staining with Ki67 antibody (16A8, BioLegend). Flow cytometry analysis was performed with BD Fortessa (BD Biosciences), and data were analyzed with FlowJo software (Treestar).

Mixed lymphocyte reaction—B6 CD4$^+$ T cells were purified using a negative selection kit from the spleen, as described above. T cells were labeled with CellTrace violet proliferation dye (Invitrogen) and co-cultured in a 1:1 ratio with BALB/c splenocytes treated with mitomycin-C (25 μg/ml) (Thermo-Fischer). Cell proliferation was analyzed on day 7 by flow cytometry.

Quantitation of mRNA and proteins—For RNA isolation, the RNeasy kit (Qiagen) was used for FACS-sorted cells; otherwise, Trizol was used. cDNA was analyzed by real-time PCR with KAPA SYBR FAST qPCR master mix (KK4605) with the primers shown in Table S1. Gene-expression levels were evaluated by the $-\Delta Ct$ method with *Actb* as an internal control. In Figures 4H, S3H, and S7A, error bars were calculated as RQ-Min = $2^{-(\Delta Ct + T*SD(\Delta Ct))}$ and RQ-Max = $2^{-(\Delta Ct - T*SD(\Delta Ct))}$ from triplicate wells as suggested by a manufacturer of PCR machines (Applied Biosystems). T*SD(ΔCt) is

a square root of x^2+y^2, where x and y are standard deviations of Ct values for a gene of interest and internal control, respectively. RQ-MIN and RQ-MAX are the acceptable errors for a 95% confidence limit according to Student's t-test. The results shown are representative of multiple independent experiments with similar results. To evaluate cytokine serum concentrations, LEGENDplex mouse T helper cytokine panel (BioLegend) was used. sOPN ELISA was performed as previously described (Shinohara et al., 2005).

Histological score analysis—Colons and SI were flushed with HBSS/10mM HEPES and cut open longitudinally. Swiss rolls were made by holding the end of the intestine/colon using a wooden stick and rolling them over until the end. Rolls were fixed in 10% formalin for 24 hrs, dehydrated, and embedded in paraffin; 5 μm thick sections were prepared. Paraffin-embedded formalin-fixed sections were stained with Hematoxylin/eosin (H/E) staining. Pathology scores were determined in a blinded manner by a pathologist based on villi blunting, crypt loss and regeneration, epithelial cell apoptosis, immune cell infiltrates, and mucosal ulceration of lamina propria (0.5, focal and rare; 1, focal and mild; 2, diffuse and mild; 3, diffuse and moderate; 4, diffuse and severe).

Tissue immunofluorescence staining and imaging—Swiss rolls for SI and colons were fixed and dehydrated in 30% sucrose for 24 hrs before embedding and freezing in the Tissue-Tek O.C.T. compound (4583, Sakura). Tissues were sectioned using a Cryostar NX50 (Thermo Fisher Scientific) at 5 μm for staining with antibodies (listed in Key resources Table) with ProLong™ Gold Antifade Mountant with DAPI (P36930, Invitrogen). Slides were imaged on spinning disk AndorDragonfly confocal microscope and images were quantified using ImageJ at 25 μm depth as Z-stacks. For quantifications, 7-8 fields/sections were captured in two sections/samples using the 20x objective and analyzed using ImageJ (Schindelin et al., 2012).

***Ex vivo* cell death analysis with precision-cut intestinal slices (PCIS)—**PCIS were prepared as previously described (de Graaf et al., 2010). Briefly, one end of the SI was tied using a suture and the remaining segment was inflated with 2.5% low melting-point agarose. Inflated SI was kept at 4°C to solidify agarose. Small cylinders of inflated SI (4 cm) were transferred to a pre-cooled cylinder mold plunger on Compresstome (VF-200-0Z, Precisionary) to cut the 400 μm thick slices. Slices were transferred to complete William's medium and pre-incubated with 10 μg/ml of CD44 antibody (listed in Key resources Table) for the first 3 hrs followed by the addition of 50 ng/ml of recombinant mouse OPN (763602, BioLegend) for the next 4 hrs. Slices were then incubated with 0.1 ng/ml TNF-α (575202, BioLegend) for the additional 16 hrs. Some slices were kept as control; TNFα treated. Floating slices were then stained with antibodies (listed in Key resources Table) and CF640R TUNEL (640R TUNEL Assay Apoptosis Detection Kit; 30074, Biotium) for immunofluorescence analysis.

Intenstinal permeability assay using FITC-Dextran—Mice were fasted for 3.5 hrs and, followed by oral gavage of 150 μl of 4-kDa FITC-dextran (Sigma-Aldrich) (80 mg/ml diluted in water). Five hrs later, serum samples were collected, and FITC-dextran leakage was spectrophotometrically evaluated using a Sunrise™ plate reader (Tecan).

Fecal sample collection for 16S rRNA sequencing—Fecal samples were collected from individual mice and bacterial DNA was isolated using DNeasy PowerLyzer PowerSoil Kit (Qiagen) as described by the manufacture. Fecal microbiota analysis was performed as described previously (Shahi et al., 2019). For microbial profiling, we performed amplicon sequencing by amplifying the V3-V4 region of the 16S rRNA gene using PCR primers (listed in Table S1) and barcoded using Nextera XT Index Kit (Illumina) (Shahi et al., 2019).

qPCR analysis of SI-associated bacteria—Microbial burdens of SI-associated bacteria were evaluated by qPCR by using phylum-specific 16S rRNA primers and normalized to pan-bacterial 16S rRNA primers, as described before (Guo et al., 2008; Kanayama et al., 2015; Murri et al., 2013). SI samples were flushed with PBS to remove feces before collecting samples for analysis of tissue-associated bacteria, then homogenized in Trizol using trituration with an 18G needle and syringe followed by the QIAShredder homogenizer (Qiagen). DNA extraction was then performed on Trizol samples per manufacturer protocol (ThermoFisher).

16S rRNA sequencing microbiome analysis—Fecal microbiota analysis was performed as described previously (Shahi et al., 2019). Raw 16S sequence data was processed by the DADA2 R script to generate amplicon sequence variants (ASVs) which were then assigned taxonomies using a naive Bayesian classifier with the Silva database as a reference. The phyloseq R package was used for downstream analysis and generation of Figures 4A–4C (McMurdieand Holmes, 2013). Specifically, Principle Coordinate Analysis (PCoA) was based on Bray Curtis dissimilarity metrics in Figure 4A, and the Shannon index was used to calculate alpha diversity in Figure 4B. Phyloseq and DESeq2 were used for differential abundance analysis of genus and taxa in Figures 4D–4G (Love et al., 2014). Adjusted p-values are shown in Figures 4D–4F. Differential abundance analysis data is provided in Table S2.

QUANTIFICATION AND STATISTICAL ANALYSIS

Methods of statistical data analyses, including the Student's t-test (unpaired, two-tailed in all cases), Welch's t-test, and one or two-factor analysis of variance (ANOVA), were described in figure legends. Post-hoc Sidak or Tukey multiple comparison test with repeated measures was applied if two-factor ANOVA yielded an interaction term $p < 0.1$. Log-transformation was performed before 2-factor ANOVA as appropriate when data include values that varied greatly in magnitude between multiple cell types (Figures 1G and 4I). Percent survival of mice was analyzed by the Gehan-Breslow-Wilcoxon test. Specific P values are presented for each experiment in figure legends, and $P<0.05$ is interpreted as statistically significant. Microsoft Excel or GraphPad Prism software was used for statistical analyses.

Supplementary Material

Refer to Web version on PubMed Central for supplementary material.

ACKNOWLEDGMENTS

REFERENCES

Allen RD, Staley TA, and Sidman CL (1993). Differential cytokine expression in acute and chronic murine graft-versus-host-disease. Eur. J. Immunol 23, 333–337. [PubMed: 8436168]

Ashkar S, Weber GF, Panoutsakopoulou V, Sanchirico ME, Jansson M, Zawaideh S, Rittling SR, Denhardt DT, Glimcher MJ, and Cantor H (2000). Eta-1 (osteopontin): an early component of type-1 (cell-mediated) immunity. Science 287, 860–864. [PubMed: 10657301]

Barry ST, Ludbrook SB, Murrison E, and Horgan CM (2000a). Analysis of the alpha4beta1 integrin-osteopontin interaction. Exp. Cell Res 258, 342–351. [PubMed: 10896785]

Barry ST, Ludbrook SB, Murrison E, and Horgan CM (2000b). A regulated interaction between alpha5beta1 integrin and osteopontin. Biochem. Biophys. Res. Commun 267, 764–769. [PubMed: 10673366]

Chiusolo P, Metafuni E, Paroni Sterbini F, Giammarco S, Masucci L, Leone G, and Sica S (2015). Gut microbiome changes after stem cell transplantation. Blood 126, 1953.

Coghill JM, Sarantopoulos S, Moran TP, Murphy WJ, Blazar BR, and Serody JS (2011). Effector CD4+ T cells, the cytokines they generate, and GVHD: something old and something new. Blood 117, 3268–3276. [PubMed: 21245483]

Cooke KR, Kobzik L, Martin TR, Brewer J, Delmonte J Jr., Crawford JM, and Ferrara JL (1996). An experimental model of idiopathic pneumonia syndrome after bone marrow transplantation: I. The roles of minor H antigens and endotoxin. Blood 88, 3230–3239. [PubMed: 8963063]

da Silva AP, Ellen RP, Sorensen ES, Goldberg HA, Zohar R, and Sodek J (2009). Osteopontin attenuation of dextran sulfate sodium-induced colitis in mice. Lab Invest 89, 1169–1181. [PubMed: 19668240]

Da Silva AP, Pollett A, Rittling SR, Denhardt DT, Sodek J, and Zohar R (2006). Exacerbated tissue destruction in DSS-induced acute colitis of OPN-null mice is associated with downregulation of TNF-alpha expression and non-programmed cell death. J. Cell Physiol 208, 629–639. [PubMed: 16741956]

de Graaf IA, Olinga P, de Jager MH, Merema MT, de Kanter R, van de Kerkhof EG, and Groothuis GM (2010). Preparation and incubation of precision-cut liver and intestinal slices for application in drug metabolism and toxicity studies. Nat. Protoc 5, 1540–1551. [PubMed: 20725069]

Denhardt DT, and Noda M (1998). Osteopontin expression and function: role in bone remodeling. J. Cell. Biochem. Suppl 30-31, 92–102. [PubMed: 9893260]

Ghimire S, Weber D, Mavin E, Wang XN, Dickinson AM, and Holler E (2017). Pathophysiology of GvHD and other HSCT-related major complications. Front. Immunol 8, 79. [PubMed: 28373870]

Gladson CL, and Cheresh DA (1991). Glioblastoma expression of vitronectin and the alpha v beta 3 integrin. Adhesion mechanism for transformed glial cells. J. Clin. Invest 88, 1924–1932. [PubMed: 1721625]

Guo X, Xia X, Tang R, Zhou J, Zhao H, and Wang K (2008). Development of a real-time PCR method for Firmicutes and Bacteroidetes in faeces and its application to quantify intestinal population of obese and lean pigs. Lett. Appl. Microbiol 47, 367–373. [PubMed: 19146523]

Heilmann K, Hoffmann U, Witte E, Loddenkemper C, Sina C, Schreiber S, Hayford C, Holzlohner P, Wolk K, Tchatchou E, et al. (2009). Osteopontin as two-sided mediator of intestinal inflammation. J. Cell. Mol. Med 13, 1162–1174. [PubMed: 18627421]

Heimesaat MM, Nogai A, Bereswill S, Plickert R, Fischer A, Loddenkemper C, Steinhoff U, Tchaptchet S, Thiel E, Freudenberg MA, et al. (2010). MyD88/TLR9 mediated immunopathology

and gut microbiota dynamics in a novel murine model of intestinal graft-versus-host disease. Gut 59, 1079–1087. [PubMed: 20639251]
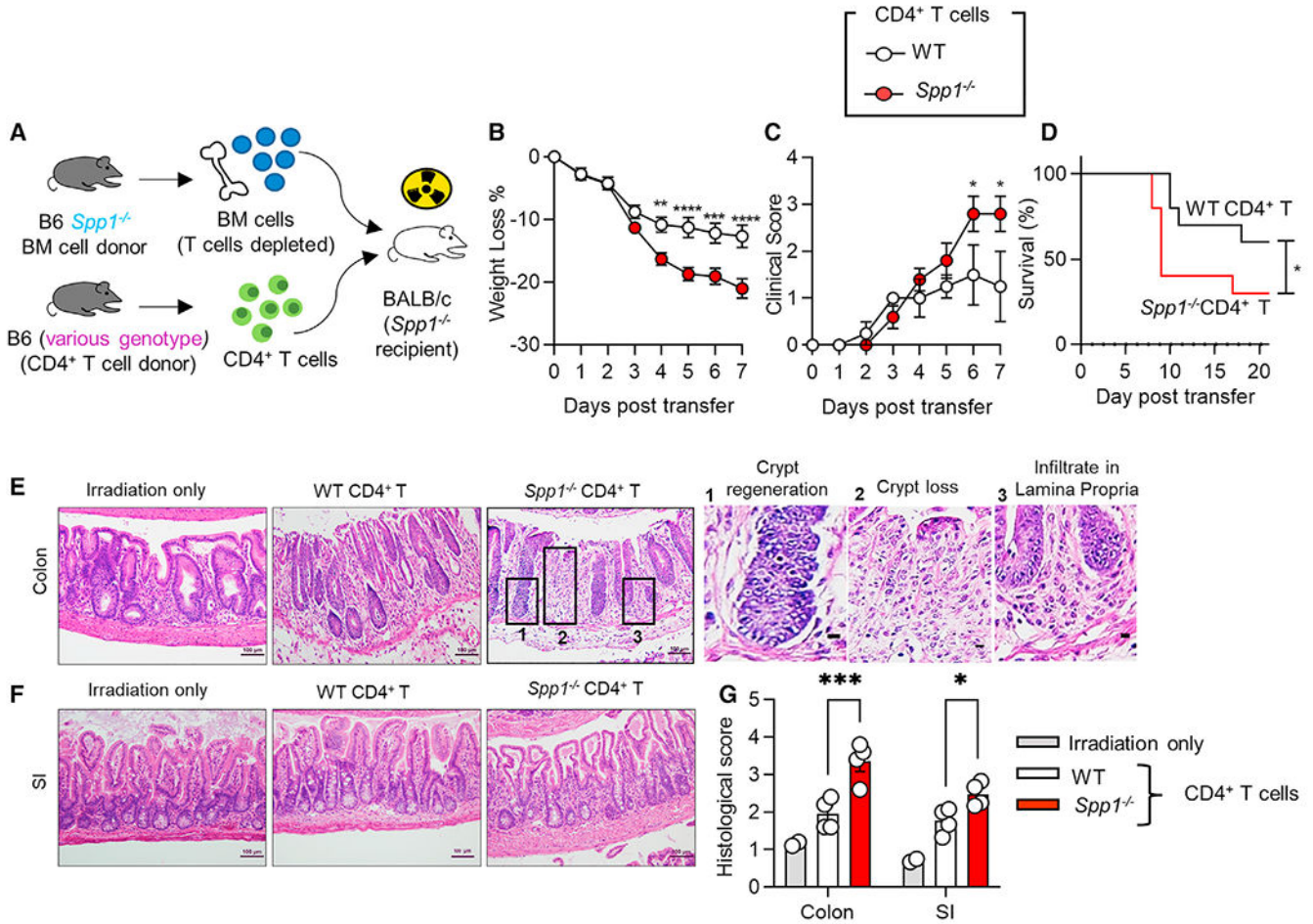
Hill GR, and Ferrara JL (2000). The primacy of the gastrointestinal tract as a target organ of acute graft-versus-host disease: rationale for the use of cytokine shields in allogeneic bone marrow transplantation. Blood 95, 2754–2759. [PubMed: 10779417]

Holler E, Butzhammer P, Schmid K, Hundsrucker C, Koestler J, Peter K, Zhu W, Sporrer D, Hehlgans T, Kreutz M, et al. (2014). Metagenomic analysis of the stool microbiome in patients receiving allogeneic stem cell transplantation: loss of diversity is associated with use of systemic antibiotics and more pronounced in gastrointestinal graft-versus-host disease. Biol. Blood Marrow Transplant. 20, 640–645. [PubMed: 24492144]

Hong T, Wang R, Wang X, Yang S, Wang W, Gao Q, and Zhang X (2021). Interplay between the intestinal microbiota and acute graft-versus-host disease: experimental evidence and clinical significance. Front. Immunol 12, 644982. [PubMed: 33815399]

Hur EM, Youssef S, Haws ME, Zhang SY, Sobel RA, and Steinman L (2007). Osteopontin-induced relapse and progression of autoimmune brain disease through enhanced survival of activated T cells. Nat. Immunol 8, 74–83. [PubMed: 17143274]

Ilett EE, Jørgensen M, Noguera-Julian M, Nørgaard JC, Daugaard G, Helleberg M, Paredes R, Murray DD, Lundgren J, MacPherson C, et al. (2020). Associations of the gut microbiome and clinical factors with acute GVHD in allogeneic HSCT recipients. Blood Adv. 4, 5797–5809. [PubMed: 33232475]

Inoue M, Arikawa T, Chen YH, Moriwaki Y, Price M, Brown M, Perfect JR, and Shinohara ML (2014). T cells down-regulate macrophage TNF production by IRAK1-mediated IL-10 expression and control innate hyperinflammation. Proc. Natl. Acad. Sci. U S A 111, 5295–5300. [PubMed: 24706909]

Inoue M, Moriwaki Y, Arikawa T, Chen YH, Oh YJ, Oliver T, and Shinohara ML (2011). Cutting edge: critical role of intracellular osteopontin in antifungal innate immune responses. J. Immunol 186, 19–23. [PubMed: 21135164]

Inoue M, and Shinohara ML (2011). Intracellular osteopontin (iOPN) and immunity. Immunol. Res 49, 160–172. [PubMed: 21136203]

Inoue M, and Shinohara ML (2015). Cutting edge: role of osteopontin and integrin alphav in T cell-mediated anti-inflammatory responses in endotoxemia. J. Immunol 194, 5595–5598. [PubMed: 25972484]

Jansson M, Panoutsakopoulou V, Baker J, Klein L, and Cantor H (2002). Cutting edge: attenuated experimental autoimmune encephalomyelitis in eta-1/osteopontin-deficient mice. J. Immunol 168, 2096–2099. [PubMed: 11859094]

Kaleta B (2019). Osteopontin enhances donor-specific alloreactivity of human peripheral blood mononuclear cells. J. Pre Clin. Clin. Res 13, 106–109.

Kanayama M, He YW, and Shinohara ML (2015). The lung is protected from spontaneous inflammation by autophagy in myeloid cells. J. Immunol 194, 5465–5471. [PubMed: 25911758]

Kanayama M, Xu S, Danzaki K, Gibson JR, Inoue M, Gregory SG, and Shinohara ML (2017). Skewing of the population balance of lymphoid and myeloid cells by secreted and intracellular osteopontin. Nat. Immunol 18, 973–984. [PubMed: 28671690]

Kawakami K, Minami N, Matsuura M, Iida T, Toyonaga T, Nagaishi K, Arimura Y, Fujimiya M, Uede T, and Nakase H (2017). Osteopontin attenuates acute gastrointestinal graft-versus-host disease by preventing apoptosis of intestinal epithelial cells. Biochem. Biophys. Res. Commun 485, 468–475. [PubMed: 28192120]

Korngold R (1993). Biology of graft-vs.-host disease. Am. J. Pediatr. Hematol. Oncol 15, 18–27. [PubMed: 8447559]

Kourepini E, Aggelakopoulou M, Alissafi T, Paschalidis N, Simoes DC, and Panoutsakopoulou V (2014). Osteopontin expression by CD103-dendritic cells drives intestinal inflammation. Proc. Natl. Acad. Sci. U S A 111, E856–E865. [PubMed: 24550510]

Leavenworth JW, Verbinnen B, Wang Q, Shen E, and Cantor H (2015a). Intracellular osteopontin regulates homeostasis and function of natural killer cells. Proc. Natl. Acad. Sci. U S A 112, 494–499. [PubMed: 25550515]

Leavenworth JW, Verbinnen B, Yin J, Huang H, and Cantor H (2015b). A p85alpha-osteopontin axis couples the receptor ICOS to sustained Bcl-6 expression by follicular helper and regulatory T cells. Nat. Immunol 16, 96–106. [PubMed: 25436971]

Lee JL, Wang MJ, Sudhir PR, Chen GD, Chi CW, and Chen JY (2007). Osteopontin promotes integrin activation through outside-in and inside-out mechanisms: OPN-CD44V interaction enhances survival in gastrointestinal cancer cells. Cancer Res 67, 2089–2097. [PubMed: 17332338]

Liang J, Huang HI, Benzatti FP, Karlsson AB, Zhang JJ, Youssef N, Ma A, Hale LP, and Hammer GE (2016). Inflammatory Th1 and Th17 in the intestine are each driven by functionally specialized dendritic cells with distinct requirements for MyD88. Cell Rep 17, 1330–1343. [PubMed: 27783947]

Love MI, Huber W, and Anders S (2014). Moderated estimation of fold change and dispersion for RNA-seq data with DESeq2. Genome Biol 15, 550. [PubMed: 25516281]

MacDonald KPA, Hill GR, and Blazar BR (2017). Chronic graft-versus-host disease: biological insights from preclinical and clinical studies. Blood 129, 13–21. [PubMed: 27821504]

McMurdie PJ, and Holmes S (2013). phyloseq: an R package for reproducible interactive analysis and graphics of microbiome census data. PLoS One 8, e61217. [PubMed: 23630581]

Murri M, Leiva I, Gomez-Zumaquero JM, Tinahones FJ, Cardona F, Soriguer F, and Queipo-Ortuño MI (2013). Gut microbiota in children with type 1 diabetes differs from that in healthy children: a case-control study. BMC Med 11, 46. [PubMed: 23433344]

Ou J, Liang S, Guo XK, and Hu X (2020). Alpha-defensins promote Bacteroides colonization on mucosal reservoir to prevent antibiotic-induced dysbiosis. Front. Immunol 11, 2065. [PubMed: 33013873]

Paczesny S (2018). Biomarkers for posttransplantation outcomes. Blood 131, 2193–2204. [PubMed: 29622549]

Patouraux S, Bonnafous S, Voican CS, Anty R, Saint-Paul MC, Rosenthal-Allieri MA, Agostini H, Njike M, Barri-Ova N, Naveau S, et al. (2012). The osteopontin level in liver, adipose tissue and serum is correlated with fibrosis in patients with alcoholic liver disease. PLoS One 7, e35612. [PubMed: 22530059]

Renkl AC, Wussler J, Ahrens T, Thoma K, Kon S, Uede T, Martin SF, Simon JC, and Weiss JM (2005). Osteopontin functionally activates dendritic cells and induces their differentiation toward a Th1-polarizing phenotype. Blood 106, 946–955. [PubMed: 15855273]

Riehl TE, Santhanam S, Foster L, Ciorba M, and Stenson WF (2015). CD44 and TLR4 mediate hyaluronic acid regulation of Lgr5+ stem cell proliferation, crypt fission, and intestinal growth in postnatal and adult mice. Am. J. Physiol. Gastrointest. Liver Physiol 309, G874–G887. [PubMed: 26505972]

Sasada R, Marumoto R, and Igarashi K (1988). Secretion of human EGF and IgE in mammalian cells by recombinant DNA techniques; use of a IL-2 leader sequence. Cell Struct. Funct 13, 129–141. [PubMed: 3260137]

Scatena M, Almeida M, Chaisson ML, Fausto N, Nicosia RF, and Giachelli CM (1998). NF-kappaB mediates alphavbeta3 integrin-induced endothelial cell survival. J. Cell Biol 141, 1083–1093. [PubMed: 9585425]

Schindelin J, Arganda-Carreras I, Frise E, Kaynig V, Longair M, Pietzsch T, Preibisch S, Rueden C, Saalfeld S, Schmid B, et al. (2012). Fiji: an open-source platform for biological-image analysis. Nat. Methods 9, 676–682. [PubMed: 22743772]

Shahi SK, Zarei K, Guseva NV, and Mangalam AK (2019). Microbiota analysis using two-step PCR and next-generation 16S rRNA gene sequencing. J. Vis. Exp 10.3791/59980.

Shinohara ML, Jansson M, Hwang ES, Werneck MB, Glimcher LH, and Cantor H (2005). T-bet-dependent expression of osteopontin contributes to T cell polarization. Proc. Natl. Acad. Sci. U S A 102, 17101–17106. [PubMed: 16286640]

Shinohara ML, Kim HJ, Kim JH, Garcia VA, and Cantor H (2008). Alternative translation of osteopontin generates intracellular and secreted isoforms that mediate distinct biological activities in dendritic cells. Proc. Natl. Acad. Sci. U S A 105, 7235–7239. [PubMed: 18480255]

Shinohara ML, Lu L, Bu J, Werneck MB, Kobayashi KS, Glimcher LH, and Cantor H (2006). Osteopontin expression is essential for interferon-alpha production by plasmacytoid dendritic cells. Nat. Immunol 7, 498–506. [PubMed: 16604075]

Shlomchik WD, Lee SJ, Couriel D, and Pavletic SZ (2007). Transplantation's greatest challenges: advances in chronic graft-versus-host disease. Biol. Blood Marrow Transplant 13, 2–10. [PubMed: 17222762]

Singh N, Inoue M, Osawa R, Wagener MM, and Shinohara ML (2017). Inflammasome expression and cytomegalovirus viremia in critically ill patients with sepsis. J. Clin. Virol 93, 8–14. [PubMed: 28550722]

Smith GE, Ju G, Ericson BL, Moschera J, Lahm HW, Chizzonite R, and Summers MD (1985). Modification and secretion of human interleukin 2 produced in insect cells by a baculovirus expression vector. Proc. Natl. Acad. Sci. U S A 82, 8404–8408. [PubMed: 3878519]

Uede T (2011). Osteopontin, intrinsic tissue regulator of intractable inflammatory diseases. Pathol. Int 61, 265–280. [PubMed: 21501293]

Vaschetto R, Nicola S, Olivieri C, Boggio E, Piccolella F, Mesturini R, Damnotti F, Colombo D, Navalesi P, Della Corte F, et al. (2008). Serum levels of osteopontin are increased in SIRS and sepsis. Intensive Care Med. 34, 2176–2184. [PubMed: 18807011]

Via CS, Rus V, Gately MK, and Finkelman FD (1994). IL-12 stimulates the development of acute graft-versus-host disease in mice that normally would develop chronic, autoimmune graft-versus-host disease. J. Immunol 153, 4040–4047. [PubMed: 7930611]

Williams KM, Hakim FT, Rosenberg A, Kleiner D, Mitchell SA, Tamm M, Avila D, Lee SJ, Halter J, Prince SS, et al. (2016). Plasma osteopontin is a biomarker specifically associated with bronchiolitis obliterans syndrome after HCT. Biol. Blood Marrow Transplant 22, S417–S418.

Wolff D, Greinix H, Lee SJ, Gooley T, Paczesny S, Pavletic S, Hakim F, Malard F, Jagasia M, Lawitschka A, et al. (2018). Biomarkers in chronic graft-versus-host disease: quo vadis? Bone Marrow Transplant. 53, 832–837. [PubMed: 29367715]

Woo SH, Lee SH, Park JW, Go DM, and Kim DY (2019). Osteopontin protects colonic mucosa from dextran sodium sulfate-induced acute colitis in mice by regulating junctional distribution of occludin. Dig. Dis. Sci 64, 421–431. [PubMed: 30146676]

Yu J, Storer BE, Kushekhar K, Abu Zaid M, Zhang Q, Gafken PR, Ogata Y, Martin PJ, Flowers ME, Hansen JA, et al. (2016). Biomarker panel for chronic graft-versus-host disease. J. Clin. Oncol 34, 2583–2590. [PubMed: 27217465]

Zeineldin M, and Neufeld K (2012). Isolation of epithelial cells from mouse gastrointestinal tract for western blot or RNA analysis. Bio Protoc 2, e292.

Zeiser R, and Blazar BR (2017). Pathophysiology of chronic graft-versus-host disease and therapeutic targets. N. Engl. J. Med 377, 2565–2579. [PubMed: 29281578]

Zhao F, Zhang Y, Wang H, Jin M, He S, Shi Y, Guo Y, and Zhang Y (2011). Blockade of osteopontin reduces alloreactive CD8+ T cell-mediated graft-versus-host disease. Blood 117, 1723–1733. [PubMed: 21119110]

Highlights

- OPN generated by allogeneic CD4$^+$ T cells limits acute GVHD, manifested in the gut

- A mouse system for conditional OPN isoform-specific production is developed

- sOPN, not iOPN, protects IECs from cell death

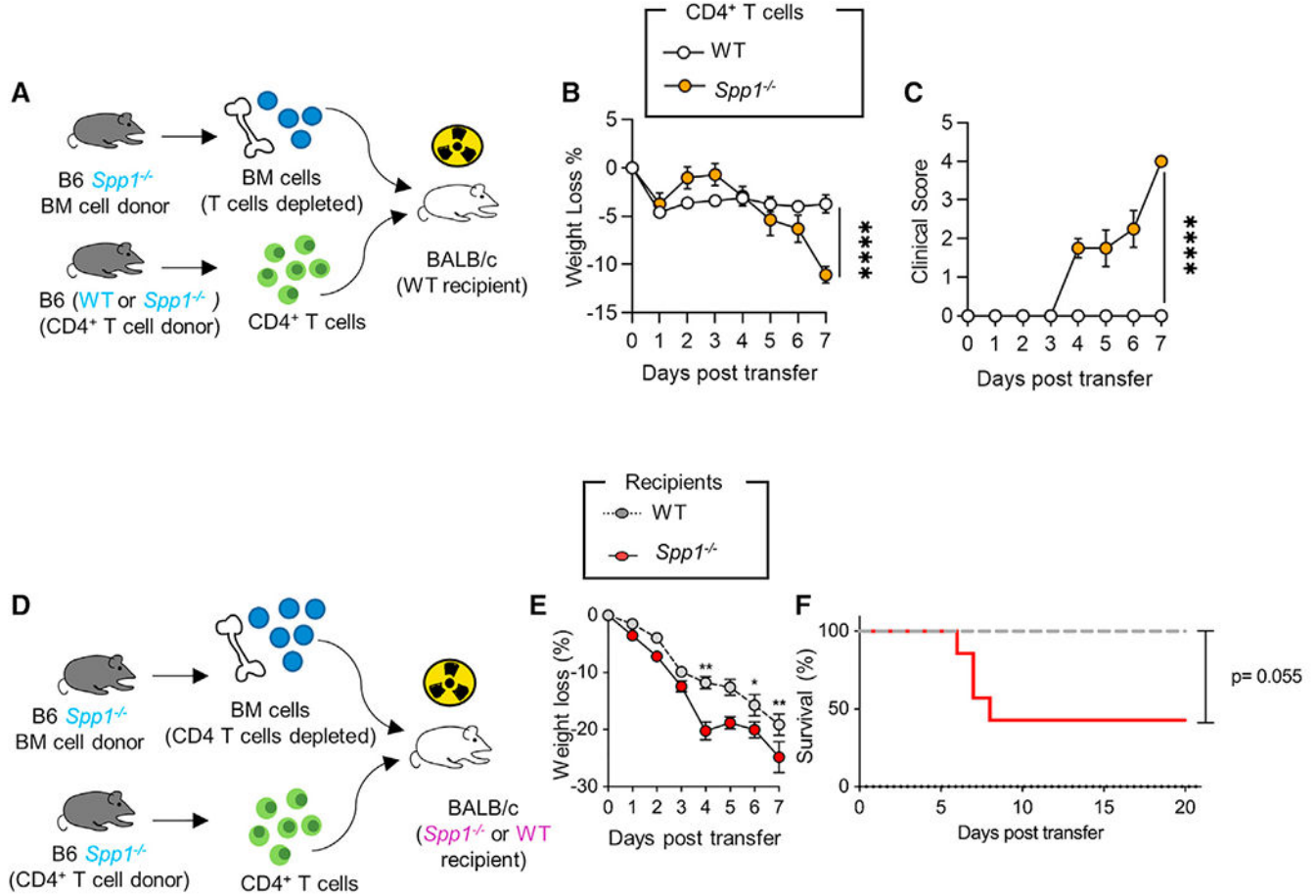- CD44 mediates sOPN's protective role in acute GVHD

Figure 1. CD4+ T cell-derived OPN is protective in aGVHD

(A) Schematic diagram of aGVHD induction. Recipient mice were BALB/c *Spp1*−/−, lethally irradiated before transferring B6 CD4+ T cells of various genotypes and T cell-depleted *Spp1*−/− B6 BM cells. This protocol was used for almost all the experiments unless otherwise noted.

(B–G) Comparison of aGVHD severity between recipients with WT (n = 13) or *Spp1*−/− (n = 14) CD4+ T cells. Weight loss (B), clinical score (C), and survival (D) were evaluated. Data are combined from three independent experiments. Representative images of hematoxylin-eosin (H&E) staining of the colon (E) and SI (F) with histology scores (G) on day 7 after adoptive cell transfer.

Recipients of WT or *Spp1*−/− CD4+ T cells (n = 4 mice/group), alongside control mice (irradiation only) (n = 2 mice/group), were compared. Insets in (E) depict (1) crypt regeneration, (2) crypt loss, and (3) lamina propria infiltrates in the colon from *Spp1*−/− CD4+ T cell recipients. Scale bars, 100 μm (10 μm for insets 1–3). Quantitative data were analyzed using two-way ANOVA followed by *post hoc* Sidak multiple comparison test (B and C) or Tukey's multiple comparison test (G) with repeated measures. Percentage survival (D) was analyzed by the Gehan-Breslow-Wilcoxon test. Data are shown as mean ± SEM. *p < 0.05, **p < 0.01, ***p < 0.001, ****p < 0.0001.

Figure 2. Donor CD4⁺ T cell-derived OPN is protective even with host-derived OPN

(A–C) Comparison of aGVHD severity between WT recipients with WT (n = 4) or *Spp1⁻/⁻* (n = 4) CD4⁺ T cells. Experimental schematics (A), weight loss (B), and survival (C) are shown. Results are representative of three independent experiments.

(D–F) Comparison of aGVHD severity between WT and *Spp1⁻/⁻* recipients. Experimental schematics depicting *Spp1⁻/⁻* CD4⁺ T cells and T cell-depleted *Spp1⁻/⁻* BM being transferred to indicated recipients (D). Weight loss (E) and survival (F) are shown. Results are combined from two independent experiments using n = 12 mice/group for both groups. Statistical analyses were performed using two-way ANOVA followed by a *post hoc* Sidak multiple comparison test (B, C, and E) with repeated measures. Percentage survival (F) was analyzed by the Gehan-Breslow-Wilcoxon test. Data are shown as mean ± SEM. *p < 0.05, **p < 0.01, ***p < 0.001, ****p < 0.0001. See also Figure S3.
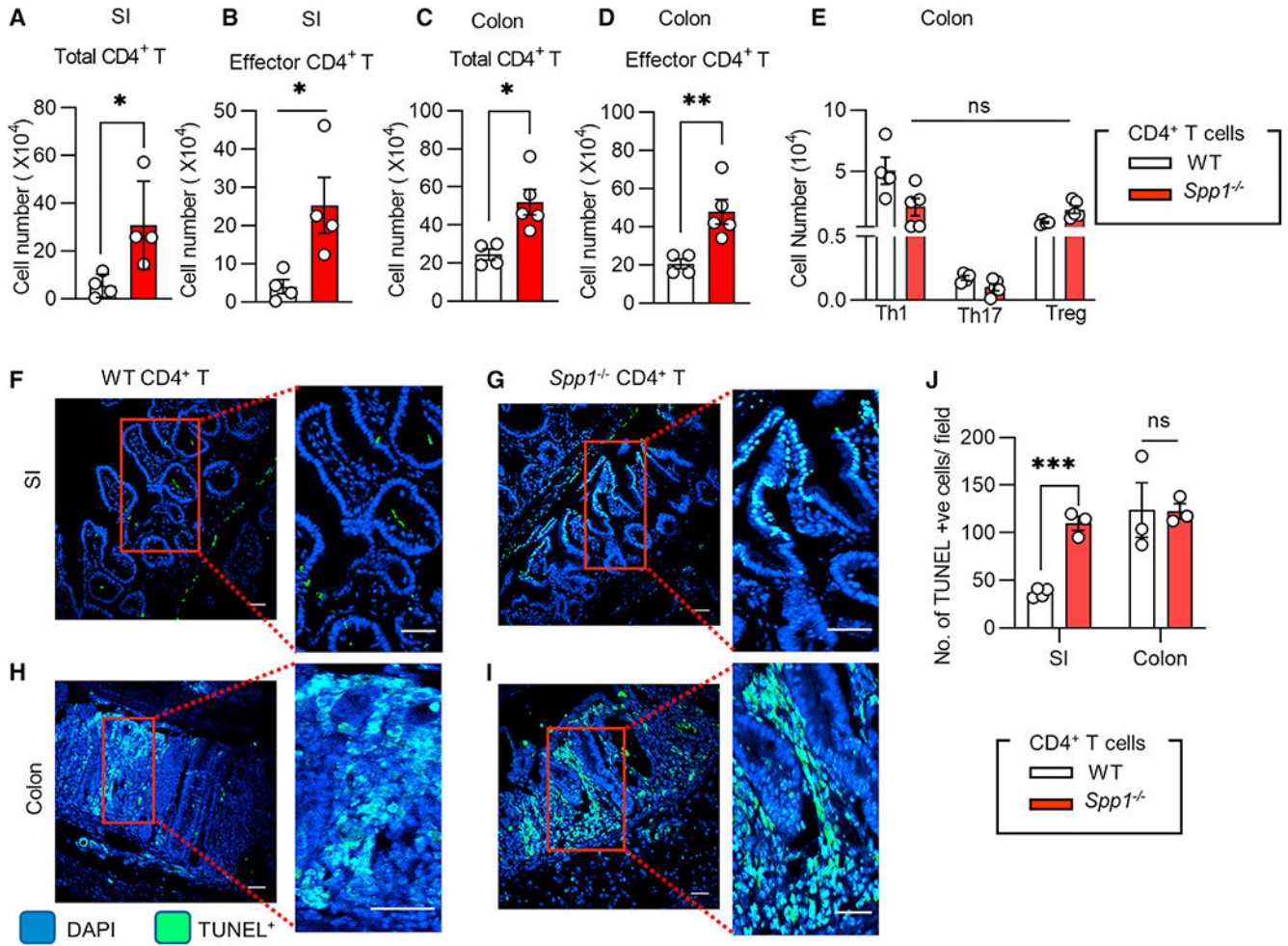
Figure 3. CD4+ T cell-derived OPN limits T cell infiltration in the gut and cell death in the GI tract during aGVHD

aGVHD was induced as described in Figure 1A, and the recipients were analyzed on day 7 after adoptive cell transfer.

(A and B) Cell numbers of total CD4+ T (A) and CD44+CD62L−CD4+ T effector (B) cells in SI. n = 4 mice/group.

(C–E) Cell numbers of total CD4+ T (C), CD44+CD62L−CD4+ T effector (D), and indicated T_H cell subsets (E) in the colon. Results are representative of two independent experiments. One data point denotes a value from one mouse. Recipients of WT (n = 4) or *Spp1−/−* CD4+ T cells (n = 5).

(F–J) Representative images of TUNEL staining in SI (F and G) and colon (H and I), comparing recipients with transferred CD4+ T cells of WT (F and H) versus *Spp1−/−* (G and I). Scale bar, 50 μm. (J) Quantification of TUNEL+ cell staining in SI and colon. Eight fields per mouse were analyzed, and the average of TUNEL-positive cells per field was denoted as one data point per mouse. SI data are from n = 4 mice with WT CD4+ T cells and n = 3 mice with *Spp1−/−* CD4+ T cells. Colon data are from n = 3 mice for both groups. Statistical analyses were performed using an unpaired two-tailed t test (A–D) or two-way ANOVA (E

and J) followed by a *post hoc* Sidak multiple comparison test with repeated measures. Data are shown as mean ± SEM. *p < 0.05, **p < 0.01, ***p < 0.001.
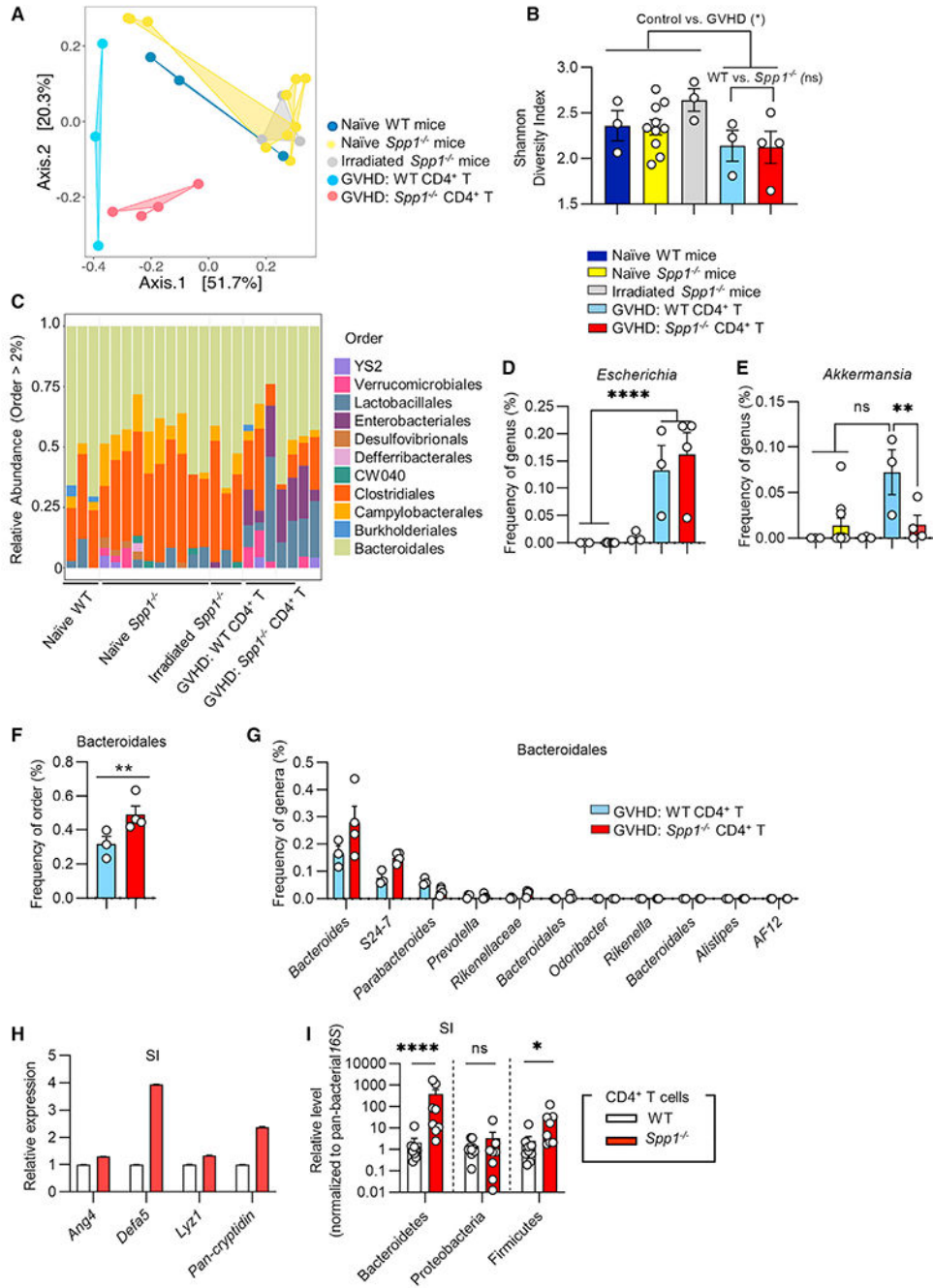
Figure 4. CD4+ T cell-mediated OPN correlates with increased commensal bacteria, *Akkermansia*, and reduced levels of epithelium-associated Bacteroidetes

(A–G) Bacterial 16S rRNA sequencing was performed to identify bacterial microbiome. aGVHD was induced as depicted in Figure 1A. Fecal samples were obtained 7 days after adoptive cell transfer. Control groups include naive BALB/c WT and *Spp1*−/− mice, in addition to irradiated BALB/c *Spp1*−/− mice without any adoptive cell transfer. Data presented are principal coordinate analysis (PCoA) plots (A), the Shannon diversity index (B), and the relative abundance of bacteria (C–G). Frequencies indicated are at bacterial order (C and F) and genus (D, E, and G) levels. Naive WT and irradiated mouse groups, n =

3; naive $Spp1^{-/-}$ mouse group, n = 10; GVHD with WT CD4$^+$ T cells, n = 3; GVHD with $Spp1^{-/-}$ CD4$^+$ T cells, n = 4. Statistical analyses (A–G) were performed as described in the STAR Methods. Adjusted p values from differential abundance analysis; **padj < 0.002.

(H) Host gene expression in the SI from mice with aGVHD, induced as shown in Figure 1A, at 7 days after adoptive T cell transfer. cDNA from five mice were pooled as one sample, and error bars (too short to see) were calculated as RQ-MIN and RQ-MAX, as described in STAR Methods. Two independent experiments showed similar results.

(I) Bacterial burdens, on day 7 after adoptive T cell transfer, determined by 16S rRNA gene qPCR at the phylum level in SI tissue samples from mice with aGVHD, induced as shown in Figure 1A. Data are shown as mean ± SEM and statistical analyses were performed with two-way ANOVA. One data point denotes a value from one mouse (A, B, D–G, and I). *p < 0.05, ****p < 0.0001. See also Tables S1 and S2.
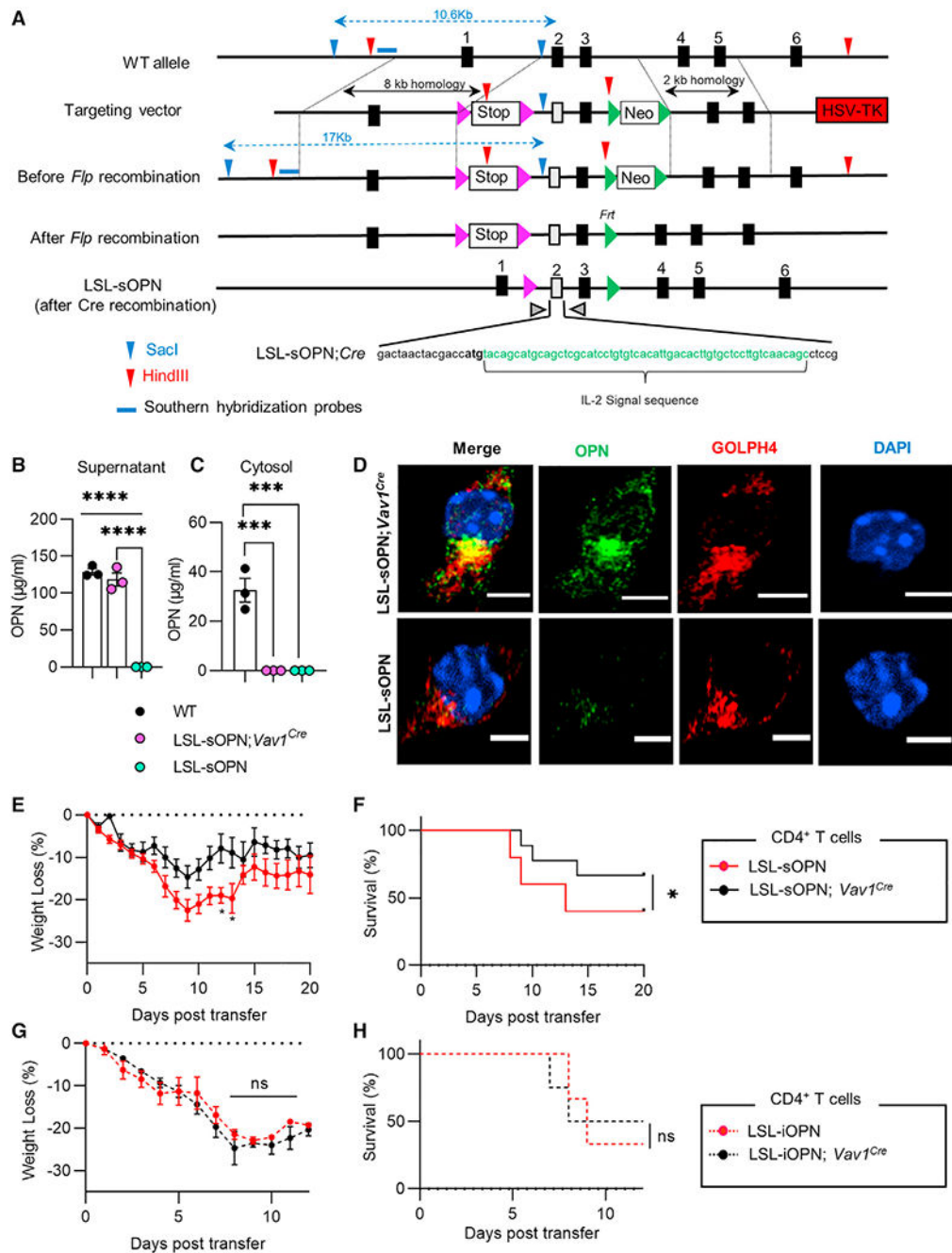
Figure 5. New mutant mouse system identified sOPN, not iOPN, by CD4+ T cells is protective in aGVHD

(A) Genomic mutation to generate LSL-sOPN mice. Black and gray boxes indicate *Spp1* exons (only the first five exons are shown). The *Spp1* signal sequence in exon 2 was replaced by the *Il2* signal sequence (57 nt, marked in green text). The targeted mutation allows the generation of sOPN alone without iOPN generation.

(B and C) Functional validation of sOPN secretion using BMDMs from WT, LSL-sOPN, and LSL-sOPN;*Vav1Cre* mice. OPN concentrations in cell culture supernatants (B) and the

cytoplasmic fraction (C) were analyzed by ELISA. The NE-PER kit was used to isolate the cytoplasm. Each data point was obtained from a value from one mouse (n = 3).

(D) Representative confocal images showing co-localization of OPN (green) with a Golgi body marker, GOLPH4 (red), in LSL-sOPN; *Vav1^Cre* (upper) BMDMs. Nuclei are stained with DAPI (blue). Scale bar, 5 μm.

(E–H) Comparison of aGVHD mice that received LSL-sOPN; *Vav1^Cre* (n = 9 mice) or LSL-sOPN (n = 10 mice) CD4$^+$ T cells. Weight loss (E) and survival (F) are shown.

(G and H) Comparison of aGVHD mice that received LSL-iOPN; *Vav1^Cre* (n = 4 mice) or LSL-iOPN (n = 4 mice) CD4$^+$ T cells. Weight loss (G) and survival (H) are shown.

aGVHD induction was performed as depicted in Figure 1A (E–H). Statistical analyses were performed using unpaired two-tailed t test (B and C) or two-way ANOVA followed by *post hoc* Sidak multiple comparison tests (E and G). Statistical analysis of survival (F and H) was performed with the Gehan-Breslow-Wilcoxon test. Data are shown as mean ± SEM. *p < 0.05, ***p < 0.001, ****p < 0.0001. See also Figure S5.
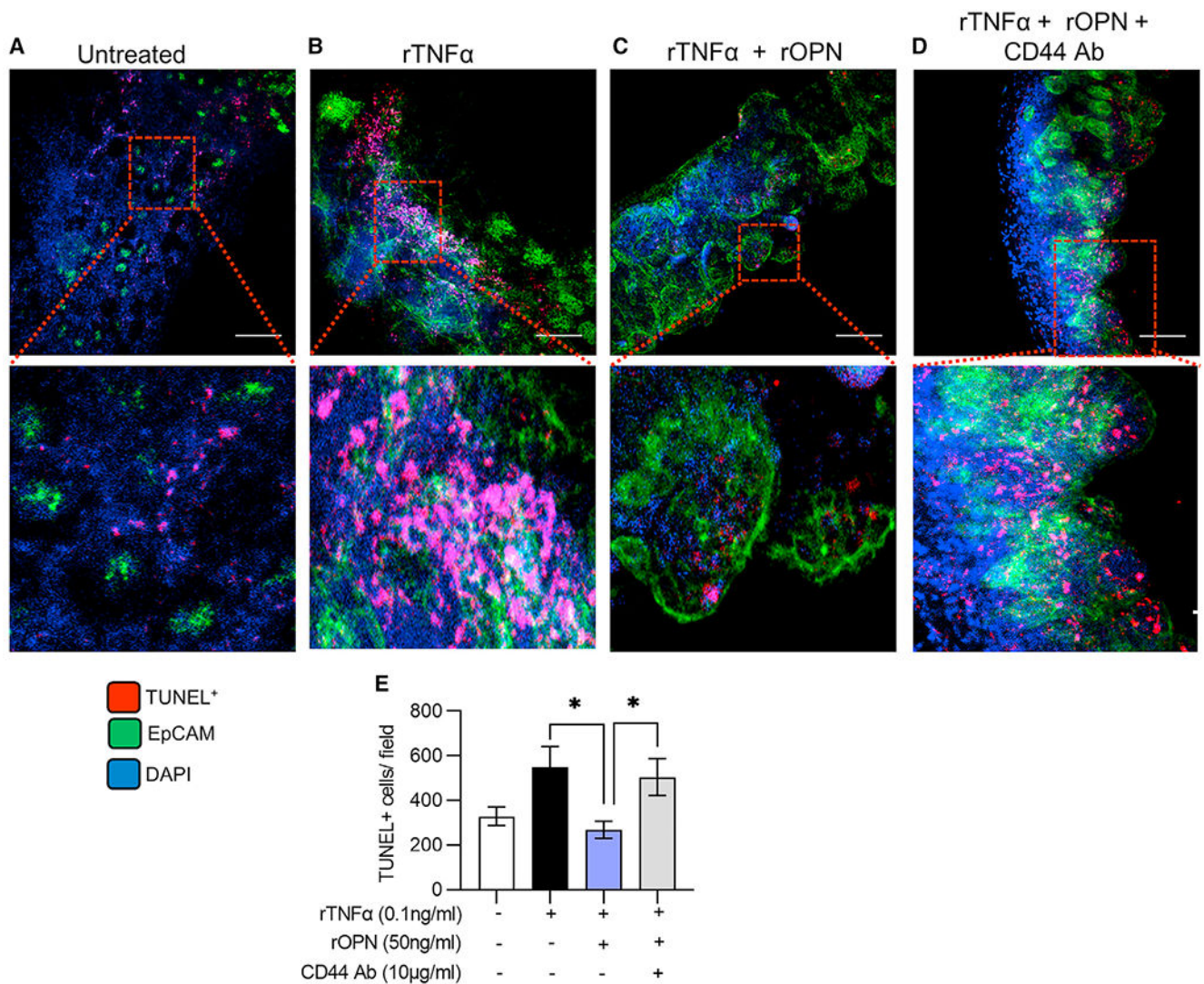
Figure 6. sOPN limits cell death of IECs in *ex vivo* PCIS

(A–D) Representative TUNEL staining images of live issue slices prepared from SI of BALB/c *Spp1*−/− mouse. PCIS were untreated (A); treated with rTNF-α alone (B); treated with rTNFα and rOPN (C); or treated with rTNFα, rOPN, and CD44 Ab (D). Scale bar, 50 μm. Results are representative of two independent experiments using two mice per experiment. Eight fields per mouse were analyzed.

(E) Quantification of TUNEL-positive cells. Statistical analyses were performed using a one-way ANOVA followed by a *post hoc* Tukey's multiple comparison test. Data are shown as mean ± SEM. *$p < 0.05$.

KEY RESOURCES TABLE

REAGENT OR RESOURCES	SOURCE	IDENTIFIER
Antibodies		
Rat monoclonal anti-CD3e (clone 145-2C11)	BioLegend	Cat#100306; RRID:AB_312671
Rat monoclonal anti-CD4 (clone GK1.5)	BioLegend	Cat#100451; RRID:
Rat monoclonal anti-CD8 (clone 53-6.7)	BioLegend	Cat#100722; RRID:AB_312761
Rat monoclonal anti-IFNγ (clone XMG1.2)	BioLegend	Cat#505806; RRID:AB_315400
Rat monoclonal anti-IL-17 (clone TC11-18H10.1)	BioLegend	Cat#506904; RRID:AB_315464
Rat monoclonal anti-Foxp3 (clone MF-14)	BioLegend	Cat#126405; RRID:AB_1089114
Rat monoclonal IgG1, k isotype control (clone RTK2071)	BioLegend	Cat#400405; RRID:AB_315381
Rat monoclonal IgG1, k isotype control (clone RTK2071)	BioLegend	Cat#400407; RRID:AB_326530
Rat monoclonal anti-CD45 (clone 30-F11)	BioLegend	Cat#103114; RRID:AB_312979
Rat monoclonal anti-CD11b (clone M1/70)	BioLegend	Cat#101257; RRID:AB_2565431
Rat monoclonal anti-CD11c (clone N418)	BioLegend	Cat#117310; RRID:AB_313779
Rat monoclonal anti-Ly6G (clone 1A8)	BioLegend	Cat#127606; RRID:AB_1236494
Rat monoclonal anti-Ly6C (clone HK1.4	BioLegend	Cat#128008; RRID:AB_1186132
Rat monoclonal anti-F4/80 (clone BM8)	BioLegend	Cat#123114; RRID:AB_893478
Rat monoclonal anti-CD45.1 (clone A20)	BioLegend	Cat#110708; RRID:AB_313497
Rat monoclonal anti-CD45.2 (clone 104)	BioLegend	Cat#109814; RRID:AB_389211
Mouse monoclonal anti-H-2K^b (clone AF6-88.5)	BioLegend	Cat#116519; RRID:AB_2721683
Mouse monoclonal anti-H-2K^d (clone AF6-88.5)	BioLegend	Cat#116629; RRID:AB_2616847
Rat monoclonal anti-CD326 (clone G8.8)	BioLegend	Cat#118204; RRID:AB_1134178
Rat monoclonal anti-CD68 (clone FA-11)	BioLegend	Cat#137003; RRID:AB_2044001
Rat monoclonal anti-CD44 (clone IM7)	BioLegend	Cat#103003; RRID:AB_312954
Hamster Anti-Mouse CD3e (clone 500A2)	BD Biosciences	Cat#553238; RRID:AB_394727
Rabbit polyclonal anti-GOLPH4/GPP130	Abcam	Cat#ab28049; RRID:AB_732692
Mouse monoclonal anti-OPN (clone AKm2A1)	Santa Cruz	Cat#SC21742; RRID:AB_219499
Streptavidin, Alexa Fluor 488 Conjugate	Thermo Fisher	Cat#S32354; RRID:AB_2315383
Goat polyclonal anti-Hamster IgG (H+L) Cross-Adsorbed Secondary Ab	Thermo Fisher	Cat#A-21110; RRID:AB_2535759
Goat polyclonal anti-rabbit (H+L) Highly Cross-Adsorbed Secondary Ab	Thermo Fisher	Cat#A-21244; RRID:AB_2535812
Goat polyclonal anti-Mouse IgG (H+L) Cross-Adsorbed Secondary Ab	Thermo Fisher	Cat#A-11029; RRID:AB_2534088
Goat polyclonal anti-OPN	R&D Systems	Cat#AF808; RRID:AB_2194992
Goat polyclonal anti-OPN	R&D Systems	Cat#BAF808; RRID:AB_2194991
Oligonucleotides		
Primers for RT qPCR; (see Table S1)	This paper	N/A
Primers for sOPN recombination; (See Table S1)	This paper	N/A
Chemicals, peptides and recombinant proteins		
Liberase enzyme	Millipore Sigma	Cat# 5401119001

REAGENT OR RESOURCES	SOURCE	IDENTIFIER
DNAse I	Sigma-Aldrich	Cat# DN25
CellTrace violet proliferation dye	Invitrogen	Cat# C34557
Mitomycin-C	Thermo-Fischer	Cat# BP25312
Recombinant mouse OPN	BioLegend	Cat# 763602
Recombinant TNF-α	BioLegend	Cat# 575202
Ionomycin (calcium salt from *Streptomyces conglobatus*)	Sigma-Aldrich	Cat# I0634
Phorbol 12-myristate 13-acetate (PMA)	Sigma-Aldrich	Cat# P1585
Prolong Gold Antifade Mountant	Thermo-Fischer	Cat# P36930
FITC-dextran	Sigma-Aldrich	Cat# 68059
Critical commercial assays		
Cytofix/Cytoperm Kit	BD	Cat# 554714
FOXP3 Fix/Perm Kit	BioLegend	Cat# 421401
CellTrace Violet Cell Proliferation Kit	Invitrogen	Cat# C34557
LIVE/DEAD Fixable Violet Dead Cell Stain Kit	Thermo-Fisher	Cat# L34955
Mouse CD4 T Lymphocyte Enrichment Set - DM	BD Biosciences	Cat# 558131
FITC-Annexin V Apoptosis Detection Kit	BioLegend	Cat# 640922
FOXP3 Fix/Perm Kit	BioLegend	Cat# 421403
Cytofix/Cytoperm kit	BD Biosciences	Cat# 554714
640R TUNEL Assay Apoptosis Detection Kit	Biotium	Cat# 30074
Experimental models: Organisms/strains		
Mouse: *Spp1*$^{-/-}$ (B6)	The Jackson Laboratory	JAX#004935
Mouse: C57BL/6J (B6)	The Jackson Laboratory	JAX#000664
Mouse: *Spp1*$^{-/-}$ (BALB/c) 129 *Spp1*$^{-/-}$ backcrossed with BALB/cJ for >14 generations	129 *Spp1*$^{-/-}$ generated by the lab of Dr. David T.Denhardt (Rutgers University). Backcrossed by our group.	N/A
Mouse: BALB/cJ	The Jackson Laboratory	JAX#000651
Mouse: *Vav1*^{cre}	The Jackson Laboratory	JAX#008610
Mouse: LSL-sOPN;	This paper	N/A
Mouse: LSL-iOPN; *Vav1*^{cre}	Generated in our lab (Kanayama et al., 2017)	N/A
Software and algorithms		
GraphPad Prism	N/A	https://www.graphpad.com/scientific-software/prism/
FlowJo	N/A	https://www.flowjo.com/solutions/flowjo
ImageJ	(Schindelin et al., 2012)	https://imagej.net/Fiji
Deposited data		
Raw and analyzed RNA-seq data for " 16s Microbiome sequencing of (GVHD) T cell recipient mice"	NCBI	PRJNA731868